Supplementary Information

Zn_2GeO_{4-x}/ZnS Heterojunctions Fabricated via in-situ Etching Sulfurization for Pt-free Photocatalytic Hydrogen Evolution: Interface Roughness and Defect Engineering

Yongli Wang,[a] Mingyue Zheng,[b] Hongkai Zhao,[b] Hao Qin,[b] Weiliu Fan,*[a] Xian Zhao[b]

[a]School of Chemistry and Chemical Engineering, Shandong University, Jinan 250100, China

[b]State Key Laboratory of Crystal Materials, Shandong University, Jinan 250100, China

Corresponding author E-mail: fwl@sdu.edu.cn

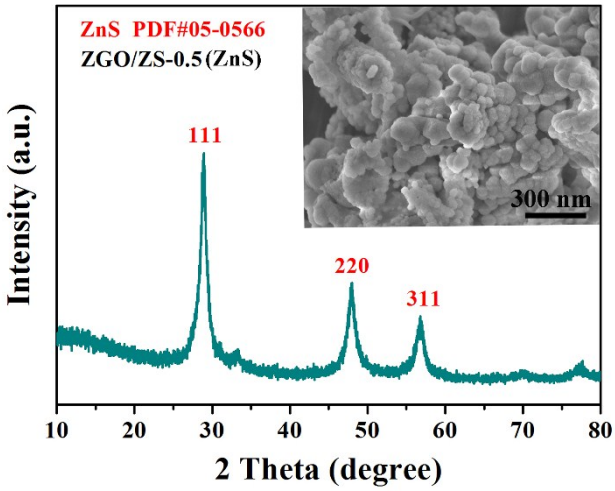

Figure S1. XRD pattern and SEM image of ZGO/ZS-0.5(ZnS) sample.

Dissolution experiment of GeO_2

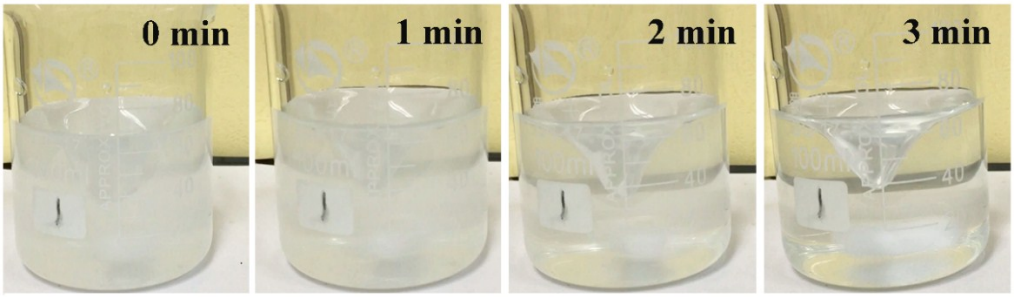

Figure S2. 150 mg GeO_2 dissolved in Na_2S solution (0.02 M) at room temperature and varies with time.

In order to indirectly verify the etching phenomenon of Zn_2GeO_4 by Na_2S solution, we added 150 mg GeO_2 into Na_2S solution (0.02 M) at room temperature. As shown in Figure S2, GeO_2 easily dissolves in Na_2S solution, which indicated that the O-Ge-O groups that are directly connected to the Zn atoms of Zn_2GeO_4 would become unstable when the Zn atoms precipitated.

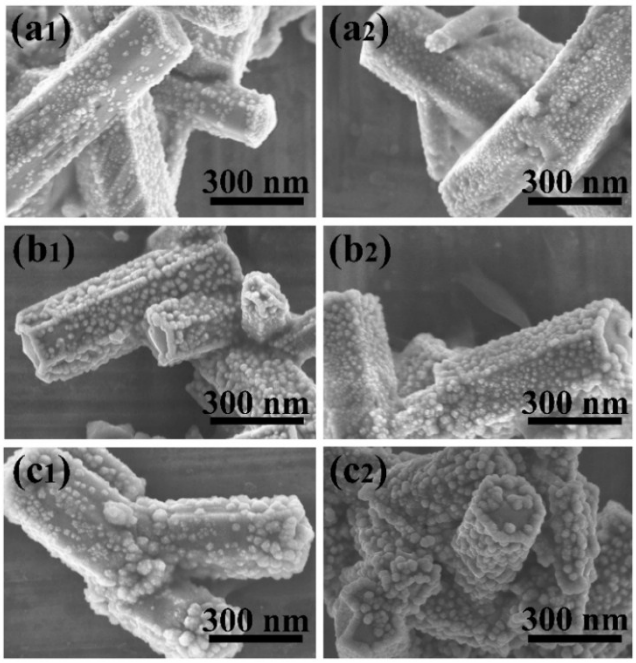

Figure S3. SEM images of the samples: (a_1) ZGO/ZS-0.01$_1$, (a_2) ZGO/ZS-0.01$_{2.5}$, (b_1) ZGO/ZS-0.02$_1$, (b_2) ZGO/ZS-0.02$_{2.5}$, (c_1) ZGO/ZS-0.04$_1$, (c_2) ZGO/ZS-0.04$_{2.5}$.

From Figure S3, we observed that the nanoparticles which dispersed on the surface of Zn_2GeO_4 became increasingly bigger with the increase of sulfurization. Prolonging the sulfurization time, more nanoparticles appeared and were well dispersed on the surface of hexagonal Zn_2GeO_4 rods. However, the nanoparticles' size was unchanged almost. Herein, we concluded that the sulfurization time is not an influencing factor for the nanoparticles' size.

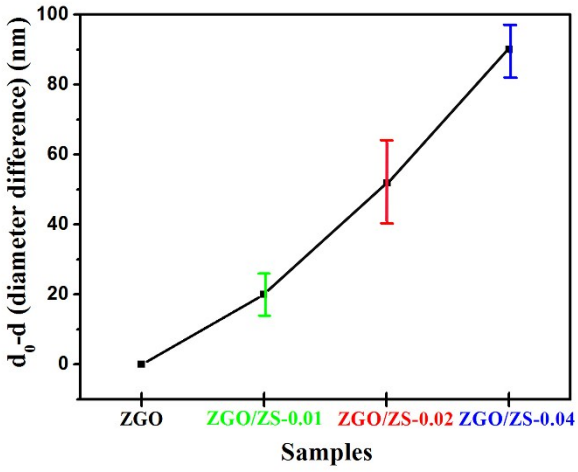

Figure S4. Diameter difference (d_0-d) of ZGO, ZGO/ZS-0.01, ZGO/ZS-0.02, ZGO/ZS-0.04 samples. (d_0 represents the diameter of catalyst rods, d represents the distribution diameter of Ge or O elements on catalyst rods)

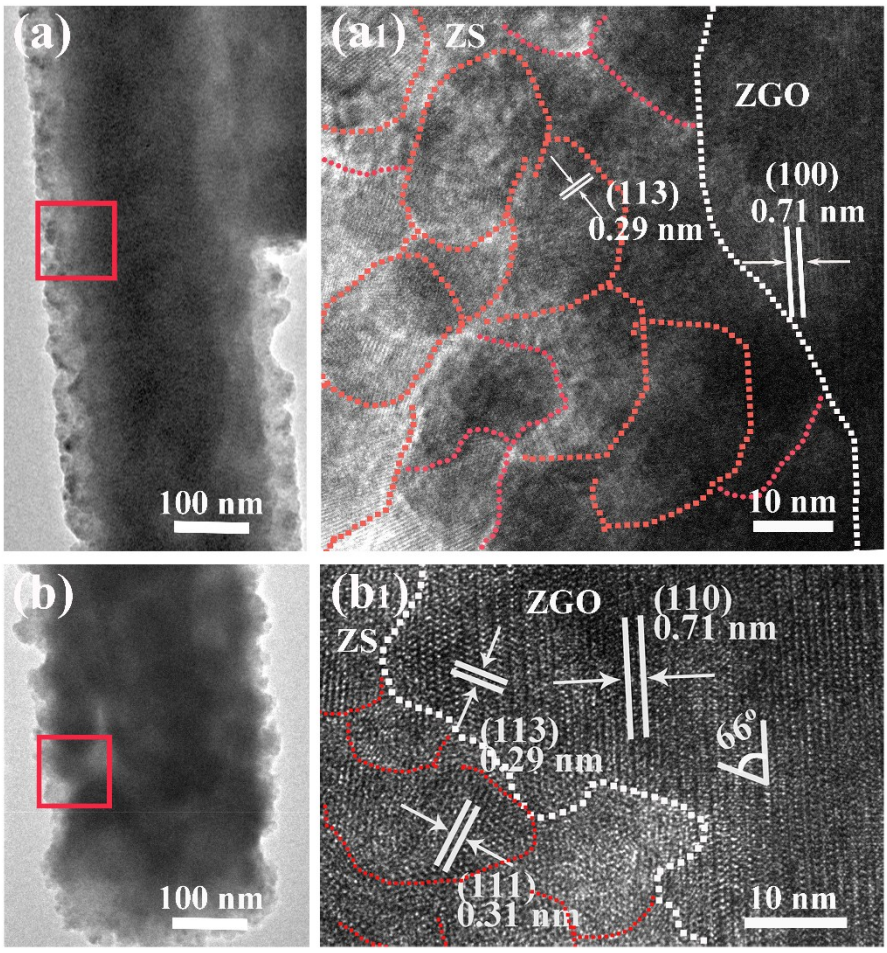

Figure S5. TEM images of the samples: (a)(b) ZGO/ZS-0.02; HRTEM images of the samples: (a_1)(b_1) ZGO/ZS-0.02.

Table S1. Concentration of Ge in the solution after the prepared ZGO/ZS heterojunctions.

Sample	**ZGO/ZS-0.01**	**ZGO/ZS-0.02**	**ZGO/ZS-0.04**	**ZGO/ZS-0.08**
Concentration	112.96 mg/L	236.34 mg/L	366.36 mg/L	459.88 mg/L

$$cos\Phi = \frac{h_1h_2 + k_1k_2 + \frac{(h_1k_2 + h_2k_1)}{2} + \frac{3a^2}{4c^2}l_1l_2}{\sqrt{(h_1^{\,2} + k_1^{\,2} + k_1h_1 + \frac{3a^2l_1^{\,2}}{4c^2})(h_2^{\,2} + k_2^{\,2} + h_2k_2 + \frac{3a^2l_2^{\,2}}{4c^2})}}$$

where the lattice parameters are: $a = 14.47$ Å, $c = 9.66$ Å.

Formula S1. Angle of crystal plane equation of hexagonal system.

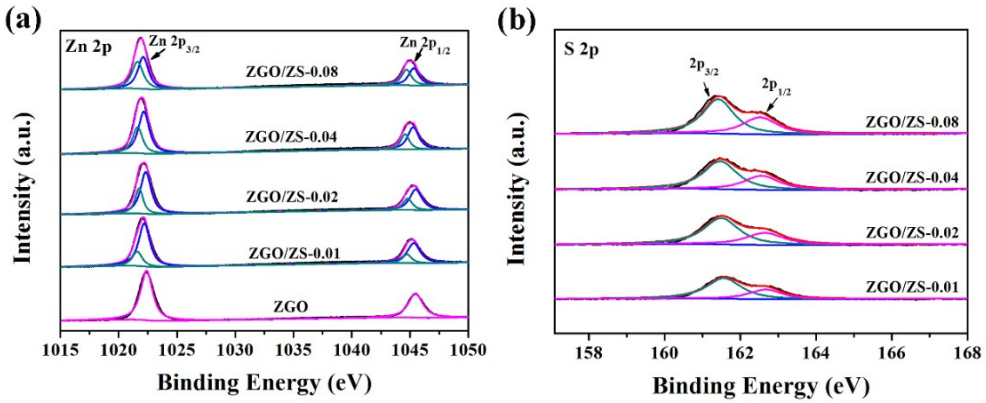

Figure S6. High resolution XPS spectra of (a) Zn 2*p* and (b) S 2*p* of ZGO, ZGO/ZS heterojunctions.

From the high-resolution XPS spectra of Zn 2*p*, we found that Zn $2p_{3/2}$ and Zn $2p_{1/2}$ peaks were both deconvoluted into two peaks in ZGO/ZS heterojunctions. The newly appeared peaks of Zn appeared at a lower binding energy compared to the pristine Zn_2GeO_4. Simultaneously, the intensity of newly appeared Zn peaks became stronger accompanied with the increase in sulfurization degree. According to the experiments, we concluded that the newly appeared Zn peaks were from ZnS. Generally, the electron density around Zn in ZnS is higher than that around Zn in Zn_2GeO_4 due to the electronegativity of O which is higher than that of S. This leads to the binding energy of Zn in ZnS being lower than the binding energy of Zn in Zn_2GeO_4.[1-3] Figure S6b shows the high-resolution XPS spectra of S 2*p*. The binding energies of S 2*p* was divided into two peaks with binding energies at 161.6 eV and 162.8 eV, corresponding to S $2p_{3/2}$ and S $2p_{1/2}$, respectively, which demonstrate the existence of S^{2-} in ZGO/ZS heterojunctions.[4,5]

Table S2. VB and CB positions and band gap of the samples.

	Band gap(eV)	**VB(V)**	**CB(V)**
ZGO	4.50	+3.25	-1.25
ZGO/ZS-0.5	3.05	+1.08	-1.97

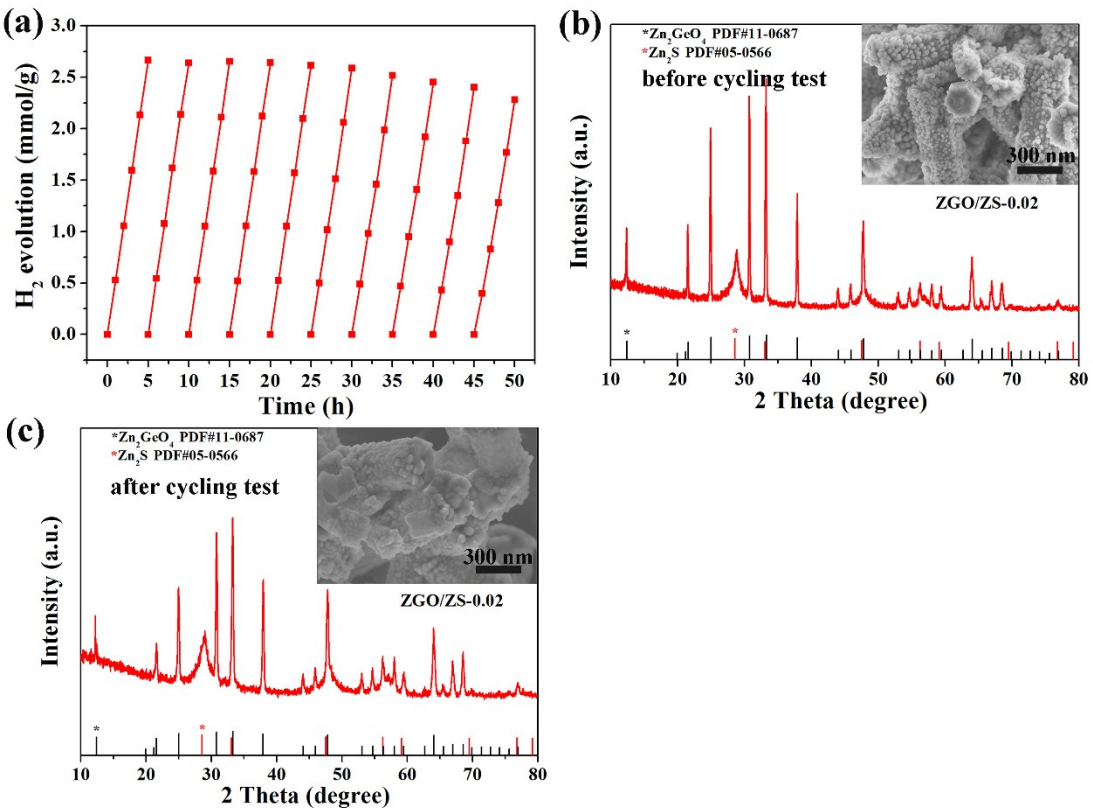

Figure S7. (a) Cycling test of ZGO/ZS-0.02; (b) XRD pattern and SEM image of ZGO/ZS-0.02 sample before cycling test; (c) XRD pattern and SEM image of ZGO/ZS-0.02 sample after cycling test.

Computational methods and model

All periodic DFT calculations were performed with the Vienna Ab initio Simulation Package (VASP) software.[6] The projector augmented wave (PAW) method was used for the treatment of core electrons, and H $1s^1$, O $2s^2$ $2p^4$, Zn $3d^{10}$ $4s^2$, and Ge $4s^2$ $4p^2$ were treated as valence electrons. The exchange correlation potential was described using the Perdew's and Wang's 1991-parameterized generalized gradient approximation.[7,8] The electron wave functions were expanded in a plane-wave basis set with a kinetic energy cut-off of 340 eV, and this cut-off energy was used throughout our calculations. The Monkhorst−Pack scheme k-point grids were 3 × 3 × 3 for the bulk unit cell and 2 × 2 × 1 for Zn_2GeO_4(100), (110), and (113) planes. The maximum forces on an atom in any direction were converged within 0.05 eV/Å to guarantee structure optimization and the convergence criterion for the total energy was set to 1×10^{-5} eV. Climbing image nudged elastic band method integrated into VASP was used to search the transition states (TS) of the reaction.[9,10] At the same

time, frequency analysis was carried out to ensure that each TS had only a single imaginary frequency.

After optimization, the calculated equilibrium structures of the lattice parameters of a unit cell of Zn_2GeO_4 were a = b = 14.17 Å, c = 9.50 Å. These values were closely aligned with experimental values (a = b = 14.23 Å, c = 9.53 Å).[11] Three surfaces of Zn_2GeO_4(100), (110), and (113) were considered in this work. These surfaces were created on the basis of an optimized bulk unit cell. The dimensions of Zn_2GeO_4(100) is 14.17 Å × 9.50 Å × 23.78 Å (seven atomic layers), which is 9.50 Å × 17.54 Å × 17.80 Å (seven atomic layers) and 21.87 Å × 8.77 Å × 17.74 Å (five atomic layers) for Zn_2GeO_4(110) and (113), respectively. During calculations, the atoms in the three topmost layers were allowed to relax, whereas the other layers were frozen.

In this paper, the adsorption energy of the water molecules were obtained by the following equation:

$$E_{ads} = E_{cat+mol} - E_{cat} - E_{mol} \quad (1)$$

where $E_{cat+mol}$ is the total energy of the Zn_2GeO_4 plane after molecular adsorption, E_{cat} is the energy of the Zn_2GeO_4 plane, and the E_{mol} is the energy of a gas phase molecule. Hence, the negative value of E_{ads} shows an exothermic process, whereas a positive value represents an endothermic process.

The reaction energy and activation barrier were calculated as:

$$E_r = E_{fin} - E_{ini} \quad (2)$$

$$E_a = E_{TS} - E_{ini} \quad (3)$$

where E_{ini}, E_{fin}, and E_{TS} represent the energy of the initial state, final state, and transition state, respectively.

The formation energy of an oxygen vacancy was calculated as

$$E_{f(Vo)} = E(D - Zn_2GeO_4) - E(Zn_2GeO_4) + \frac{1}{2}\mu(O_2) \quad (4)$$

where $E(D-Zn_2GeO_4)$ is the total energy of the defective Zn_2GeO_4 plane, $E(Zn_2GeO_4)$ is the energy of the perfect surface, and $\mu(O_2)$ is the energy of the O_2 molecule.

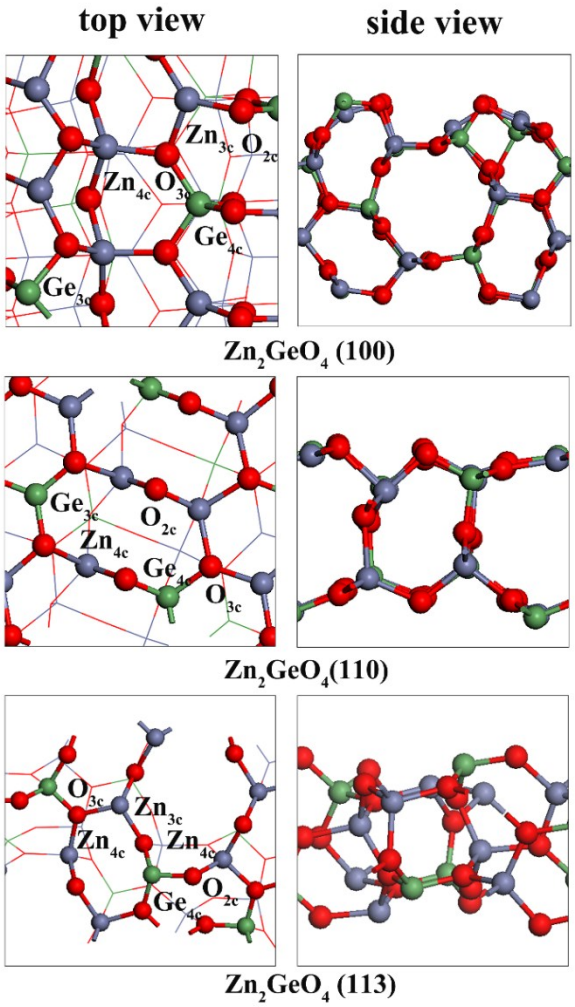

Figure S8. Top and side views of perfect Zn_2GeO_4(100), Zn_2GeO_4(110), and Zn_2GeO_4(113) planes. Purple, green, and red balls represent Zn, Ge, and O atoms, respectively.

The configurations of perfect Zn_2GeO_4(100), (110), and (113) planes in our calculations are shown in Figure S8. The outermost atoms of the Zn_2GeO_4(100) plane are fourfold coordinated Zinc (Zn_{4c}), threefold coordinated Zinc (Zn_{3c}), fourfold coordinated Germanium (Ge_{4c}), threefold coordinated Germanium (Ge_{3c}), two fold coordinated oxygen (O_{2c}), and threefold coordinated oxygen (O_{3c}). The amount of Zn_{3c} is obviously more than the amount of Ge_{3c} atoms. Low-coordinate metal atoms Zn_{3c} and Ge_{3c} is active. The type of exposed atoms on Zn_2GeO_4(110) is the same as

that of Zn_2GeO_4(100), but the number of Ge_{3c} is more than that of Zn_{3c}. On the matte Zn_2GeO_4(113) plane, there are no Ge_{3c} atoms. The defective surfaces were built by removing the O_{2c} or O_{3c} atoms on the surfaces.

Summary of different defective planes

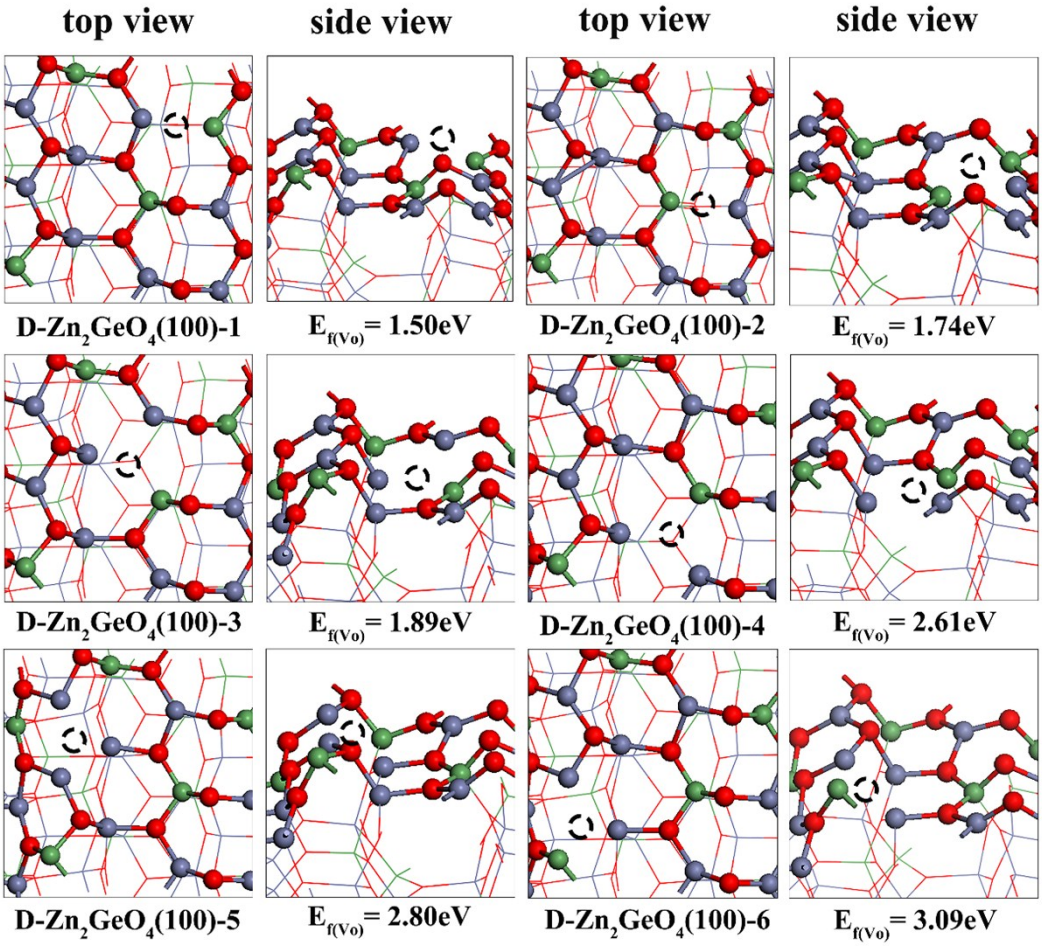

Figure S9. Top and side views of the defective Zn_2GeO_4(100) plane with different oxygen vacancies. Purple, green, and red balls represent Zn, Ge, and O atoms, respectively. Black dotted circles indicate the oxygen vacancies.

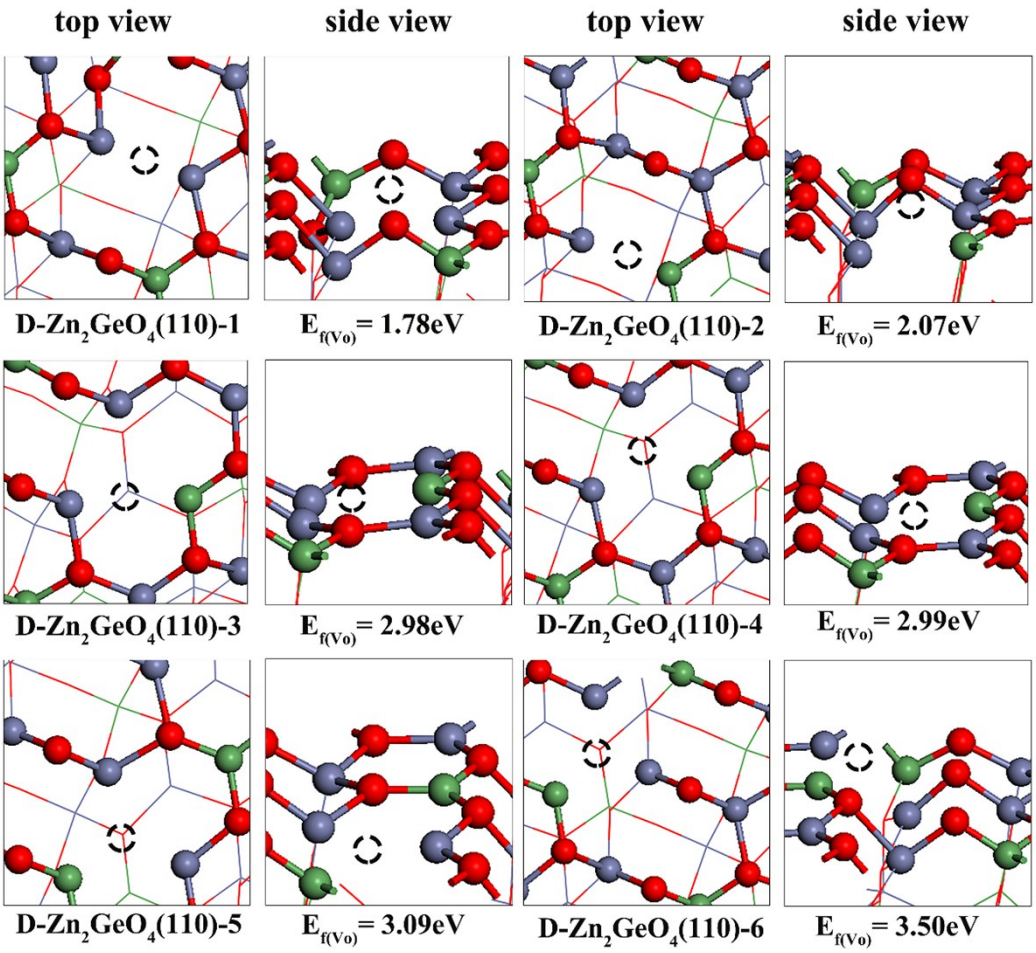

Figure S10. Top and side views of the defective $Zn_2GeO_4(110)$ plane with different oxygen vacancies. Purple, green, and red balls represent Zn, Ge, and O atoms, respectively. Black dotted circles indicate the oxygen vacancies.

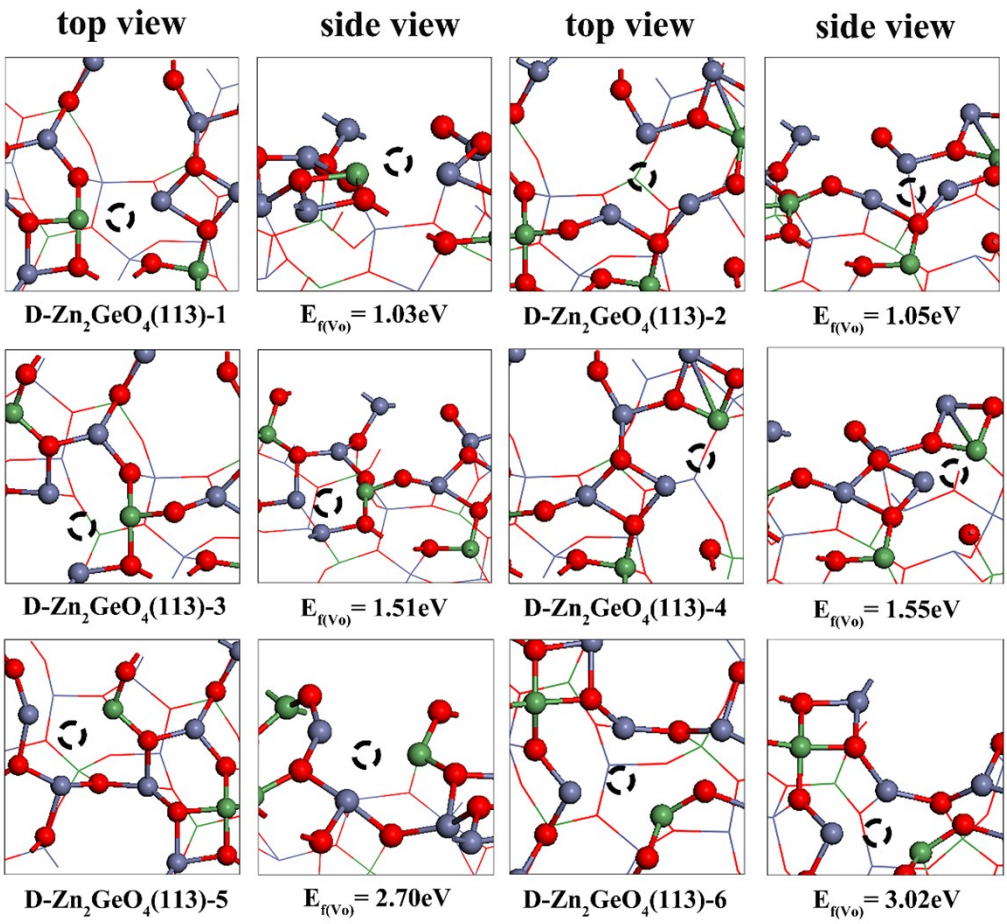

Figure S11. Top and side views of the defective $Zn_2GeO_4(113)$ plane with different oxygen vacancies. Purple, green, and red balls represent Zn, Ge, and O atoms, respectively. Black dotted circles indicate the oxygen vacancies.

References

1 A. Giannakas, E. Seristatidou, Y. Deligiannakis, I.J.A.C.B.E. Konstantinou, *Applied Catalysis B: Environmental*, 2013, **132**, 460-468.

2 B.A. Aragaw, C.-J. Pan, W.-N. Su, H.-M. Chen, J. Rick, B.-J.J.A.C.B.E. Hwang, *Applied Catalysis B: Environmental*, 2015, **163**, 478-486.

3 M.V. Dozzi, L. Artiglia, G. Granozzi, B. Ohtani, E.J.T.J.o.P.C.C. Selli, *The Journal of Physical Chemistry C*, 2014, **118**, 25579-25589.

4 G. Sun, S. Mao, D. Ma, Y. Zou, Y. Lv, Z. Li, C. He, Y. Cheng, J.-W.J.J.o.M.C.A. Shi, *Journal of Materials Chemistry A*, 2019, **7**, 15278-15287.

5 D. Jiang, Z. Sun, H. Jia, D. Lu, P.J.J.o.M.C.A. Du, *Journal of Materials Chemistry A*, 2016, **4**, 675-683.

6 G. Kresse, J. Furthmuller, *Physical Review B*, 1996, **54**, 11169-11186.

7 J.P. Perdew, J.A. Chevary, S.H. Vosko, K.A. Jackson, M.R. Pederson, D.J. Singh, C. Fiolhais, *Physical Review B*, 1992, **46**, 6671-6687.

8 J.P. Perdew, Y. Wang, *Physical Review B*, 1992, **45**, 13244.

9 G. Mills, H. Jonsson, G.K. Schenter, *Surface Science*, 1995, **324**, 305-337.

10 G. Henkelman, B.P. Uberuaga, H. Jonsson, *Journal of Chemical Physics*, 2000, **113**, 9901-9904.

11 W. Zhao, C. Zhang, Y. Shi, R. Wu, B. Zhang, *Dalton Transactions*, 2015, **44**, 75-82.